

Laser-Irradiated CrI_3 : When Chiral Photons Meet Topological Magnons

S. A. Owerre¹

¹*Perimeter Institute for Theoretical Physics,
31 Caroline St. N., Waterloo, Ontario N2L 2Y5, Canada.*

(Dated: January 12, 2022)

Abstract

Insulating honeycomb ferromagnet CrI_3 has recently attracted considerable attention due to its potential use for dissipationless spintronics applications. Recently, topological spin excitations have been observed experimentally in bulk CrI_3 by L. Chen, et al. [Phys. Rev. X **8**, 041028 (2018)] using inelastic neutron scattering. This suggest that bulk CrI_3 has strong spin-orbit coupling and its spin Hamiltonian should include a next-nearest neighbour Dzyaloshinskii-Moriya (DM) interaction. Inspired by this experiment, we study non-equilibrium emergent photon-dressed topological spin and thermal Hall transports in laser-irradiated CrI_3 with and without the DM interaction. We show that the spin excitations can be manipulated into different topological phases with different Chern numbers. Most importantly, we show that the emergent photon-dressed spin and thermal Hall response can be switched to different signs. Hence, the generated magnon spin photocurrents can be manipulated by the laser field, which is of great interest in ultrafast spin current generation and could pave the way for future applications of CrI_3 to topological opto-spintronics and opto-magnonics.

I. INTRODUCTION

In traditional modern electronic devices, Joule heating caused by the flow of electron charge (electric current) is inevitable. It can lead to large information losses. This debilitating problem can be circumvented by utilizing the electron spin degree of freedom which interacts with each other in magnetically ordered materials. In this respect, magnons (quantized collective excitations of electron spins) play a pivotal role as the primary underlying magnetic spin excitations in insulating magnetically ordered materials. They are neutral quasiparticles and carry an intrinsic spin of 1 and a spin magnetic dipole moment $\sim g\mu_B\sigma$, where g is the spin g-factor and μ_B is the Bohr magneton with $\sigma = \pm 1$. Magnon spintronics aims to eliminate the debilitating problem posed by modern electronic devices by utilizing the spin current carried by magnons as information carriers [1–10].

The recent discovery of intrinsic ferromagnetism in van der Waals crystals CrI_3 down to monolayer limit [11, 12] has garnered considerable interest in potential two-dimensional (2D) magnet-based applications, such as ultrathin magnetic sensors and high-efficiency spin filter devices [13–19]. Recently, the magnetic spin excitations in the bulk ($T_c \sim 61$ K) and monolayer ($T_c \sim 45$ K) CrI_3 have been measured by inelastic neutron scattering [33] and Raman spectroscopy [34] respectively at zero magnetic field. Both experiments have identified two distinct spin wave (magnon) modes which constitute the underlying magnetic excitations in CrI_3 . In the bulk structure, the two spin wave modes are separated by a finite energy gap $\Delta_{\mathbf{K}} \sim 4$ meV at the Dirac points [33], while the magnon bandwidth is $\Delta_{\mathbf{\Gamma}} \sim 19$ meV. The gap at the Dirac points can only be explained by the presence of the Dzyaloshinskii-Moriya interaction (DM) interaction [20–22], which breaks the inversion symmetry of the lattice resulting in the time-reversal symmetry breaking of the spin wave modes. The consequence of this result is that the spin wave modes now carry finite Berry curvatures and Chern number protected edge modes. Therefore, thermal Hall effect [23–29] can be manifested in bulk CrI_3 .

The manipulation of magnon spin currents [30–32] is essentially difficult at equilibrium, which limits the potential practical applications of topological insulating magnets in spintronics. Recently, laser-irradiation of solid-state materials has attracted considerable attention as an alternative way for engineering topological nontrivial states from topologically trivial quantum materials [35–44]. However, there are very limited applications to real ma-

terials [45–47]. This formalism, however, depends on coupling between the charge degree of freedom and the electric field component of the laser light through the Peierls phase, which result in non-equilibrium Floquet-engineered topological phases. In insulating magnets, the spin degree of freedom can couple to the electric field component of the laser light through different processes [48–58] such as the electric polarization [51] or the Aharonov-Casher phase [59], where the former is encoded in the latter. In this case, the resulting Floquet physics can renormalize the underlying spin Hamiltonian to stabilize magnetic phases and induce Floquet topological spin excitations. This provides a promising avenue for ultrafast spin current generation. Therefore, laser-irradiated CrI₃ could play an essential role in ultrafast magnon spin current switching, which could provide a great avenue to opto-spintronics and opto-magnonics [1–10].

In this paper, we study emergent photon-dressed topological spin and thermal Hall transport properties in laser-irradiated CrI₃. We consider the three-dimensional (3D) Heisenberg spin Hamiltonian for bulk CrI₃ motivated by recent inelastic neutron scattering experiment [33], with up to third nearest-neighbours $J_1 = 2.01$ meV, $J_2 = 0.16$ meV, and $J_3 = 0.18$ meV; an easy-axis anisotropy $K = 0.22$ meV, a DM interaction $D = 0.31$ meV, and an interlayer-exchange interaction $J_c = 0.59$ meV. We show that in the presence of a laser electric field with varying intensity E_0 of order 10^6 V/m and off-resonant photon energy of $\hbar\omega = 30$ meV, the spin excitations in CrI₃ can be manipulated into different photon-dressed topological phases with different Chern numbers. We further show that the spin and thermal Hall transports can be switched by the polarized photons. The direct implication of this switching is that the magnon spin photocurrents can be manipulated by polarized photons, which could lead to ultrafast spin-switching in CrI₃. We believe that the current results will provide an essential guide towards ultrafast spin transport properties in laser-irradiated CrI₃.

II. HEISENBERG SPIN HAMILTONIAN

Based on recent inelastic neutron scattering experiment [33], the equilibrium Heisenberg spin Hamiltonian that describes the bulk honeycomb ferromagnet CrI₃ can be written as

$$\mathcal{H} = - \sum_{\langle ij \rangle, \ell} J_{ij} \mathbf{S}_i^\ell \cdot \mathbf{S}_j^\ell + \sum_{\langle\langle ij \rangle\rangle, \ell} \mathbf{D}_{ij} \cdot \mathbf{S}_i^\ell \times \mathbf{S}_j^\ell - K \sum_{i, \ell} (S_i^{z, \ell})^2 - J_c \sum_{\langle \ell \ell' \rangle, i} \mathbf{S}_i^\ell \cdot \mathbf{S}_i^{\ell'}, \quad (1)$$

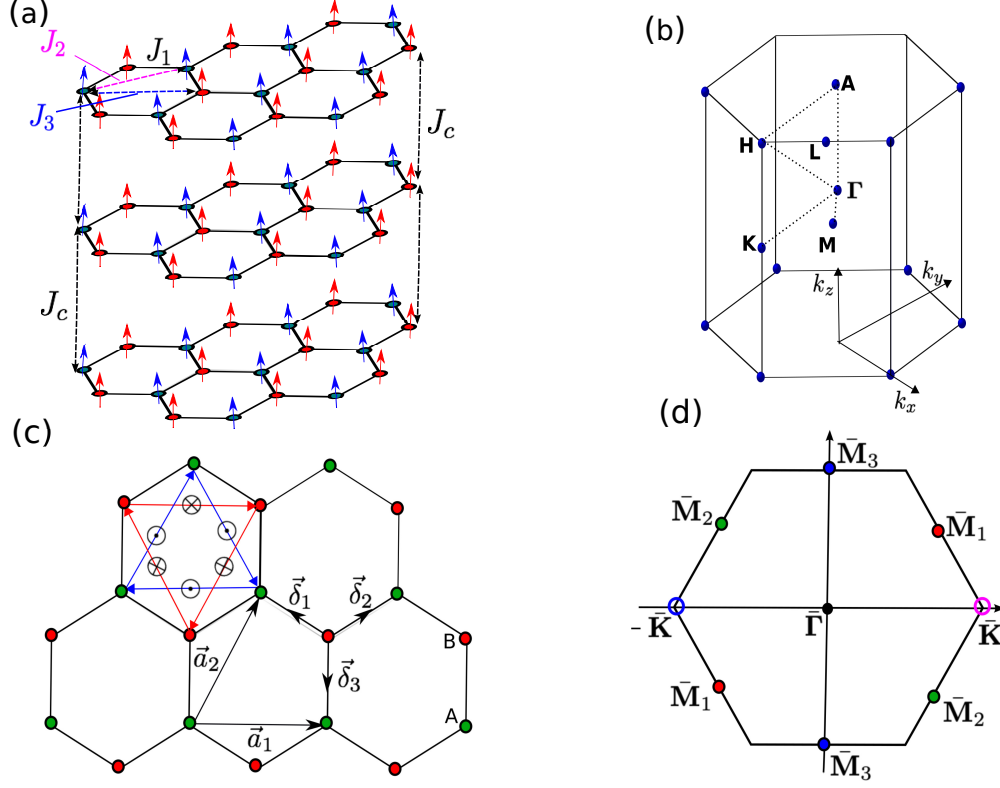


FIG. 1: Color online. (a) Bulk magnetic structure of CrI_3 with honeycomb-lattice ferromagnets stacked along the z direction. (b,d) Bulk Brillouin zone (BZ) of the lattice with high symmetry points. (c) Top view of the bulk honeycomb-lattice structure. The blue and red triangular arrows indicate the DM vector at the midpoint of the bonds. (d) Projected (001) surface BZ of the hexagonal lattice with high symmetry points.

where \mathbf{S}_i^ℓ is the spin vector at site i in layer ℓ . The first term is the intralayer Heisenberg ferromagnetic exchange interaction up to third nearest-neighbours $J_{ij} = J_1, J_2, J_3$ as depicted in Fig. 1(a). The second term is the DM interaction due to lack of inversion symmetry at the midpoint of the second-nearest-neighbour bonds as depicted in Fig. 1(c). Here $\mathbf{D}_{ij} = \nu_{ij} D \hat{\mathbf{z}}$, where $\nu_{ij} = \pm 1$ for clockwise and counter-clockwise hopping spin magnetic moments on each honeycomb layer sublattice. The third term is the easy-axis anisotropy, which forces the spins to align along the z direction in the absence of an external magnetic field. This is in stark contrast to the in-plane kagome ferromagnet $\text{Cu}(1,3\text{-bdc})$ [28, 63], where an external magnetic field is required to polarize the spins along the z axis. The fourth term is the nearest-neighbour interlayer ferromagnetic interaction between the layers. The experimentally deduced parameters are [33]: $J_1 = 2.01$ meV, $J_2 = 0.16$ meV, $J_3 = 0.18$ meV,

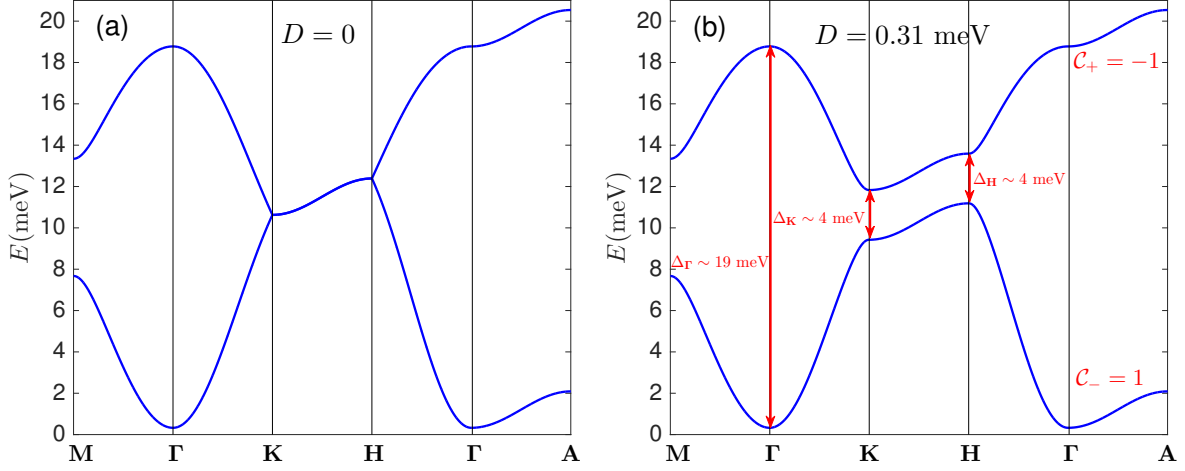


FIG. 2: Color online. Equilibrium topological magnon band structure of bulk CrI₃ for $D = 0$ (a) and $D = 0.31$ meV (b). The gap at the Dirac points is $\Delta_K = \Delta_H \sim 4$ meV in accordance with the experimentally observed Dirac gap. The magnon bandwidth is $\Delta_\Gamma \sim 19$ meV

$D = 0.31$ meV, $K = 0.22$ meV, and $J_c = 0.59$ meV.

III. THEORY OF LASER-IRRADIATED HONEYCOMB FERROMAGNET CrI₃

In the presence of an intense laser light, electron spin degree of freedom in magnetic insulators can couple to laser field through different processes [48–58]. In particular, quantized spin waves (magnons) are the oscillations of the spin magnetic dipole moment of an electron. We choose the quantization of the spin magnetic dipole moment along the z direction such that $\boldsymbol{\mu}_S = -g\mu_B\sigma\hat{\mathbf{z}}$ with $\sigma = \pm 1$. In the presence of a laser (electric) field $\mathbf{E}(\tau)$, the hopping spin magnetic dipole moments accumulate a time-dependent version of the Aharonov-Casher effect [59]

$$\Phi_{ij}(\tau) = \frac{g\mu_B}{\hbar c^2} \int_{\mathbf{r}_i}^{\mathbf{r}_j} \boldsymbol{\Xi}(\tau) \cdot d\boldsymbol{\ell}, \quad (2)$$

where $\sigma = 1$ has been used for ferromagnetic spins. $\boldsymbol{\Xi}(\tau) = \mathbf{E}(\tau) \times \hat{\mathbf{z}}$ with $\mathbf{E}(\tau) = -\partial_\tau \mathbf{A}(\tau)$, where $\mathbf{A}(\tau)$ is the time-dependent vector potential of the applied laser field. Here c is the speed of light and $\hbar = h/2\pi$ is the reduced Plank's constant. We note that the electric field of the laser light $\mathbf{E}(\tau)$ can also couple to spin degree of freedom through the electric

polarization (magnetoelectric coupling) as in multiferroics [48, 50, 51]. In both cases, the coupling between the spin degree of freedom and the electric field of the laser light can result in a laser-induced scalar spin chirality (or spin-orbit interaction) when only first nearest-neighbour hopping is considered.

As an alternative method, we can consider the charge degree of freedom, which also couples to a laser field as in Mott insulators [60, 61]. In this case, the electrons accumulate the Peierls phase

$$\varphi_{ij}(\tau) = \frac{e}{\hbar} \int_{\mathbf{r}_i}^{\mathbf{r}_j} \mathbf{A}(\tau) \cdot d\boldsymbol{\ell}, \quad (3)$$

where e is the electron charge. We note that both phases in Eqs. (2) and (3) originate from the same space-homogeneous electric field of a laser light. The dimensionless quantities that characterize the light intensity in Eqs. (2) and (3) are $\alpha_m = g\mu_B E_0 a / \hbar c^2$ and $\alpha_e = e E_0 a / \hbar \omega$ respectively, where a is the lattice constant. Therefore, the duality relation $\alpha_m = \alpha_e$ yields

$$g\mu_B = \frac{ec\lambda}{2\pi}, \quad (4)$$

where λ is the light wavelength. We note that Eq. (4) is only valid for time-dependent electric field of a laser light. It does not hold for spatially varying time-independent electric field [62].

The relation in Eq. (4) implies that the spin magnetic dipole moment $g\mu_B$ carried by magnons in periodically driven magnetic insulators can be tuned by the light wavelength λ . In fact, it is comparable to the electron charge e for a typical experimentally feasible light wavelength of order 10^{-8}m . This shows that the two formalisms can be equivalent. In fact, the resulting effect of both phases in Eqs. (2) and (3) on magnetic insulators with only first nearest-neighbour hopping parameter is a laser-induced scalar spin chirality or DM interaction [56, 60, 61].

A. Light propagation along the z -direction

For light propagation along the z -direction, we choose the time-periodic vector potential $\mathbf{A}(\tau)$ such that the corresponding time-dependent electric field is given by

$$\boldsymbol{\Xi}(\tau) = E_0 [\sin(\omega\tau), \sin(\omega\tau + \phi), 0], \quad (5)$$

where E_0 is the amplitude of the electric field, ω is the angular frequency of light and ϕ is the phase difference. For circularly-polarized light $\phi = \pi/2$ and for linearly-polarized light $\phi = 0$ or π .

The electron spin magnetic dipole couples to the laser electric field through the Aharonov-Casher phase, in the same way the electron charge couples through the Peierls phase. Thus, the resulting time-dependent Heisenberg spin Hamiltonian is given by

$$\begin{aligned} \mathcal{H}(\tau) = & - \sum_{ij,\ell} J_{ij} \left[S_i^{z,\ell} S_j^{z,\ell} + \frac{1}{2} (S_i^{+, \ell} S_j^{-, \ell} e^{i\Phi_{ij,\ell}(\tau)} + \text{H.c.}) \right] \\ & + \frac{D}{2} \sum_{\langle\langle ij \rangle\rangle, \ell} \nu_{ij,\ell} (i S_i^{+, \ell} S_j^{-, \ell} e^{i\Phi_{ij,\ell}(\tau)} + \text{H.c.}) \\ & - K \sum_{i,\ell} (S_i^{z,\ell})^2 - J_c \sum_{\langle\ell\ell'\rangle, i} \mathbf{S}_i^{\ell} \cdot \mathbf{S}_i^{\ell'}, \end{aligned} \quad (6)$$

where $S_i^{\pm, \ell} = S_i^{x,\ell} \pm i S_i^{y,\ell}$ denote the spin raising and lowering operators. Note that the interlayer coupling is not affected by light propagation along the z -direction. The spin current can be derived as $J^S = \partial \mathcal{H}(\tau) / \partial \Phi_{ij,\ell}(\tau) \equiv \sum_{j \in i} j_{ij,\ell}^S$. For $D = 0$, the spin current is given by $j_{ij,\ell}^S = -i \frac{J_{ij}}{2} e^{i\Phi_{ij,\ell}(\tau)} S_i^{-, \ell} S_j^{+, \ell} + \text{H.c.}$. Thus, the time-dependent Aharonov-Casher phase $\Phi_{ij}(\tau)$ acts as a vector potential or gauge field to the spin current. In the off-resonant limit, when the photon energy is greater than the energy scale of the static system, the effective static Hamiltonian is given by [38, 41] $\mathcal{H}_{eff} \approx \mathcal{H}_0 + \Delta \mathcal{H}_{eff}$, where $\Delta \mathcal{H}_{eff} = [\mathcal{H}_1, \mathcal{H}_{-1}] / \hbar \omega$ is the photon emission and absorption term. The first term \mathcal{H}_0 is the original time-independent spin Hamiltonian with renormalized interactions $J_{ij}^{\perp} \rightarrow J_{ij}^{\perp} \mathcal{J}_0(\alpha_m)$ for $S^x S^x$ and $S^y S^y$ couplings, $J_{ij}^z \rightarrow J_{ij}$ for $S^z S^z$ coupling, and $D \rightarrow D \mathcal{J}_0(\alpha_m)$, where $\mathcal{J}_n(x)$ is the Bessel function of order n . For dominant J_1 interaction, the second term yields a photoinduced DM interaction is of the form [51, 56–58] $\Delta \mathcal{H}_{eff} \propto D_F \sum_{\langle\langle ij \rangle\rangle} \nu_{jk} \mathbf{S}_i \cdot (\mathbf{S}_j \times \mathbf{S}_k)$, where $\mathbf{S}_i = S_i^z \hat{e}_z$, $D_F \propto \sqrt{3} \sin \phi J_1^2 \mathcal{J}_1^2(\alpha_m) / \hbar \omega$. The photoinduced DM interaction arises from the commutation relation $[S_{\alpha}^{+} S_{\beta}^{-}, S_{\rho}^{+} S_{\gamma}^{-}] = 2(\delta_{\beta\rho} S_{\beta}^z S_{\alpha}^{+} S_{\gamma}^{-} - \delta_{\alpha\gamma} S_{\alpha}^z S_{\rho}^{+} S_{\beta}^{-})$, which means that J_2 and J_3 will also have a small contribution, but the dominant contribution comes from the J_1 term. Thus, the resulting static effective spin Hamiltonian in the present model comprises a photoinduced DM interaction (scalar spin chirality) and a renormalized intrinsic DM interaction which competes with each other. The spin-wave excitations of this static effective spin Hamiltonian can be captured by performing linear spin wave theory directly from Eq. (6) and taking the off-resonant limit.

We note that below the Curie temperature $T < T_c = 61$ K, the spin wave excitations in CrI_3 can be captured in linear spin wave theory by performing the linearized Holstein Primakoff transformation

$$S_i^{z,\ell} = S - a_i^{\dagger,\ell} a_i^\ell, \quad S_i^{+,\ell} \approx \sqrt{2S} a_i^\ell = (S_i^{-,\ell})^\dagger, \quad (7)$$

where $a_i^{\dagger,\ell}(a_i^\ell)$ are the bosonic creation (annihilation) operators. The resulting time-dependent linear spin-wave Hamiltonian in momentum space can be written as

$$\mathcal{H}(\tau) = E_{MF} + \sum_{\mathbf{k}} \psi^\dagger(\mathbf{k}) \cdot \mathcal{H}(\mathbf{k}, \tau) \cdot \psi(\mathbf{k}), \quad (8)$$

where E_{MF} is the mean-field energy, $\psi^\dagger(\mathbf{k}) = (a_{\mathbf{k},A}^\dagger, a_{\mathbf{k},B}^\dagger)$ is the basis vector, and $\mathbf{k} = (k_x, k_y, k_z)$ is the 3D momentum vector. The momentum space Hamiltonian is given by

$$\mathcal{H}(\mathbf{k}, \tau) = S \begin{pmatrix} \rho(k_z) + \rho_D(\mathbf{k}_\parallel, \tau) + \rho_2(\mathbf{k}_\parallel, \tau) & \rho_1(\mathbf{k}_\parallel, \tau) + \rho_3(\mathbf{k}_\parallel, \tau) \\ \rho_1^\dagger(\mathbf{k}_\parallel, \tau) + \rho_3^\dagger(\mathbf{k}_\parallel, \tau) & \rho(k_z) + \rho_D(-\mathbf{k}_\parallel, \tau) + \rho_2(\mathbf{k}_\parallel, \tau) \end{pmatrix}. \quad (9)$$

The prefactor corresponds to $S = 3/2$ for CrI_3 , and $\mathbf{k}_\parallel = (k_x, k_y)$ is the in-plane momentum wave vector.

$$\rho(k_z) = 3(J_1 + J_3) + 2K + 6J_2 + 2J_c(1 - \cos k_z) \quad (10)$$

$$\begin{aligned} \rho_1(\mathbf{k}_\parallel, \tau) = & -J_1 [e^{-i\mu_m \Xi(\tau) \cdot \delta_3} + e^{-i\mathbf{k}_\parallel \cdot \mathbf{a}_2} e^{-i\mu_m \Xi(\tau) \cdot \delta_2} \\ & + e^{-i\mathbf{k}_\parallel \cdot \mathbf{a}_1} e^{-i\mu_m \Xi(\tau) \cdot \delta_1}], \end{aligned} \quad (11)$$

$$\begin{aligned} \rho_2(\mathbf{k}_\parallel, \tau) = & -J_2 [e^{-i(\mathbf{k}_\parallel + \mu_m \Xi(\tau)) \cdot \mathbf{a}_1} + e^{-i(\mathbf{k}_\parallel + \mu_m \Xi(\tau)) \cdot \mathbf{a}_2} \\ & + e^{-i(\mathbf{k}_\parallel + \mu_m \Xi(\tau)) \cdot \mathbf{a}_3} + \text{H.c.}], \end{aligned} \quad (12)$$

$$\begin{aligned} \rho_3(\mathbf{k}_\parallel, \tau) = & -J_3 [e^{-i\mathbf{k}_\parallel \cdot (\mathbf{a}_1 + \mathbf{a}_2)} e^{-i\mu_m \Xi(\tau) \cdot 2\delta_3} \\ & + e^{i\mathbf{k}_\parallel \cdot \mathbf{a}_3} e^{-i\mu_m \Xi(\tau) \cdot (\mathbf{a}_1 + \delta_2)} + e^{-i\mathbf{k}_\parallel \cdot \mathbf{a}_3} e^{-i\mu_m \Xi(\tau) \cdot (\mathbf{a}_2 + \delta_1)}], \end{aligned} \quad (13)$$

$$\begin{aligned} \rho_D(\mathbf{k}_{\parallel}, \tau) = & -iD \left[e^{-i(\mathbf{k}_{\parallel} + \mu_m \boldsymbol{\Xi}(\tau)) \cdot \mathbf{a}_1} + e^{i(\mathbf{k}_{\parallel} + \mu_m \boldsymbol{\Xi}(\tau)) \cdot \mathbf{a}_2} \right. \\ & \left. + e^{i(\mathbf{k}_{\parallel} + \mu_m \boldsymbol{\Xi}(\tau)) \cdot \mathbf{a}_3} - \text{H.c.} \right], \end{aligned} \quad (14)$$

where $\mu_m = g\mu_B/\hbar c^2$. The nearest-neighbour vectors are given by $\boldsymbol{\delta}_1 = -(\sqrt{3}/2, 1/2)a$, $\boldsymbol{\delta}_2 = (\sqrt{3}/2, -1/2)a$, $\boldsymbol{\delta}_3 = (0, 1)a$. The primitive lattice vectors are given by $\mathbf{a}_1 = \boldsymbol{\delta}_3 - \boldsymbol{\delta}_1 = (\sqrt{3}/2, 3/2)a$, $\mathbf{a}_2 = \boldsymbol{\delta}_3 - \boldsymbol{\delta}_2 = (-\sqrt{3}/2, 3/2)a$, and $\mathbf{a}_3 = \mathbf{a}_1 - \mathbf{a}_2$.

Next, we apply the Floquet theory (see Appendix). The magnon modes at equilibrium $E_0 = 0$ are depicted in Fig. (2) with the experimentally deduced parameters for $D = 0$ (a) and $D = 0.31$ meV (b). In the former, the acoustic (lower) and the optical (upper) magnon modes form nodal line along the \mathbf{K} - \mathbf{H} line. In the latter, however, the acoustic and the optical magnon modes are well-separated due to nonzero DM interaction. In accordance with experimental observation [33], the optical magnon mode extends close to 20 meV in the $k_z = 0$ plane and the acoustic magnon mode extends up to 2 meV along the line $k_x = k_y = 0$. The small gap at the Γ point is due to nonzero easy-axis anisotropy $K = 0.22$ meV. The gap at the Dirac points at \mathbf{K} and \mathbf{H} is ~ 4 meV as observed in experiment and can be attributed to a nonzero DM interaction $D = 0.31$ meV. The acoustic and optical magnon modes carry fixed Chern number $\mathcal{C} = \pm 1$ respectively.

B. Laser-induced topological transitions in CrI_3

In our numerical calculations, we will utilize the electron spin magnetic dipole moment $\mu_B = e\hbar/2m_e$, where the g-factor has been set to 2 and m_e is the electron mass. Hence, the dimensionless intensity of light in the present formalism is $\alpha_m = eE_0a/m_e c^2$. To enhance the effect of light on the magnon bands, we consider a laser electric field amplitude of order $E_0 = \mathcal{O}(10^6 \text{ V/m})$, and set the lattice constant a to unity. Unless otherwise stated, we will use the experimentally deduced parameters for CrI_3 listed above and fix the photon energy to $\hbar\omega = 30$ meV, which is greater than the magnon bandwidth of the undriven system. In Floquet topological systems, it is customary to assume that the quasienergy levels of the Floquet Hamiltonian are close to the equilibrium system, which is realized in the off-resonant limit [35–44]. Therefore, the properties of equilibrium topological systems can be applied to Floquet topological systems.

First, we consider the laser-induced Chern number topological phase transitions of the system and focus on the lowest acoustic Floquet magnon branch. Theoretically, we can consider the 3D ferromagnetic bulk structure of CrI₃ as slices of 2D monolayer CrI₃ interpolating between the $k_z = 0$ and $k_z = \pi$ planes. For an arbitrary k_z point the Chern number of the magnon energy branches can be defined as

$$\mathcal{C}_n^F = \frac{1}{2\pi} \int_{BZ} d\mathbf{k}_{\parallel} \Omega_{n,xy}(\mathbf{k}_{\parallel}, k_z), \quad (15)$$

where $\Omega_{n,\alpha\beta}(\mathbf{k}_{\parallel}, k_z)$ is the momentum space Floquet Berry curvature for a given magnon quasienergy band n defined as

$$\Omega_{n,\alpha\beta}(\mathbf{k}) = -2\text{Im} \sum_{m \neq n} \frac{\langle u_n(\mathbf{k}) | \hat{v}_{\alpha} | u_m(\mathbf{k}) \rangle \langle u_m(\mathbf{k}) | \hat{v}_{\beta} | u_n(\mathbf{k}) \rangle}{[\varepsilon_n(\mathbf{k}) - \varepsilon_m(\mathbf{k})]^2}, \quad (16)$$

where $\hat{v}_{\alpha} = \partial \mathcal{H}_{eff}(\mathbf{k}) / \partial k_{\alpha}$ defines the velocity operators with $\alpha \neq \beta = (x, y, z)$ and $\mathcal{H}_{eff}(\mathbf{k})$ is the static effective Hamiltonian and $\varepsilon_m(\mathbf{k})$ are its Floquet quasienergies (see Appendix). For an arbitrary k_z point the Chern number is well-defined as far as the denominator in Eq. (16) is nonzero. The Chern number of all the 2D slices at an arbitrary k_z point is the same as the planes at two momenta $k_z = k_i$ and $k_z = k_i + \delta k_i$ can be adiabatically connected without closing the gap.

In Fig. (3), we have shown the evolution of the lowest Floquet Chern number as a function of electric field amplitude E_0 for $D = 0$ (a) and $D = 0.31$ meV (b). In the former, we can see that circularly-polarized light $\phi = \pi/2$ induces topological transitions in the magnon modes with the Chern number changing between $-1, +1, +2$ as E_0 varies. The sharp jump at $+2$ and -1 occur near the zeros of \mathcal{J}_0 , which renormalizes the spin interactions in the zeroth-order effective spin Hamiltonian \mathcal{H}_0 . For linearly-polarized light $\phi = 0$ and $D = 0$, the system is topologically trivial with zero Chern number because time-reversal symmetry is not broken for $\phi = 0$ and $D = 0$. In the former, however, the system is already topologically nontrivial at equilibrium $E_0 = 0$ with the Chern number $\mathcal{C} = +1$ for the lowest magnon mode. But there is no topological phase transition as the parameters are fixed. As the laser field is turned on, a topological phase transition occurs for $\phi = \pi/2$ and $\phi = 0$, with the Chern number changing between $-1, 0, +1$. Therefore, the system can be switched from a topologically nontrivial state to a topologically trivial state and back to a topologically

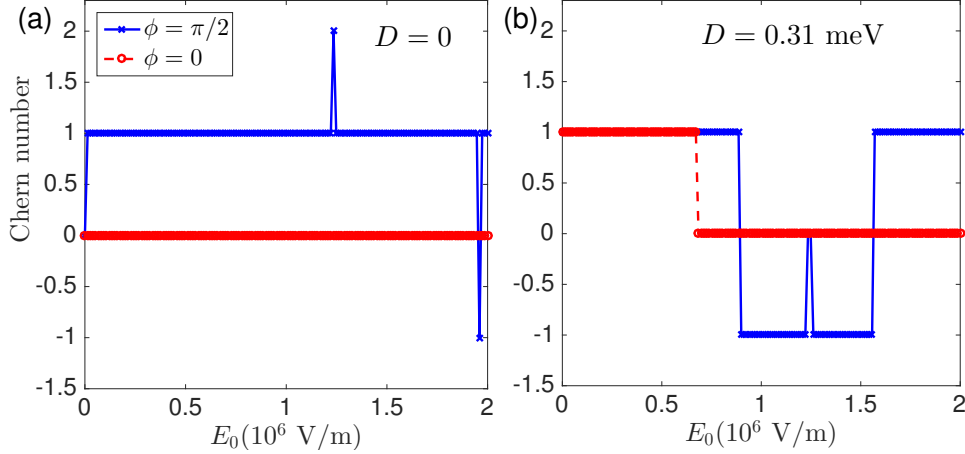


FIG. 3: Color online. Laser-induced Chern number topological phase transitions of the lowest magnon mode in CrI_3 as a function of the electric field intensity E_0 for $D = 0$ (a) and $D = 0.31$ meV (b). The photon energy is $\hbar\omega = 30$ meV.

nontrivial state for $\phi = \pi/2$. The distribution of the Chern number is accompanied by a gap closing and reopening at the $\bar{\mathbf{M}}_i$ ($i = 1, 2, 3$) and $\bar{\mathbf{K}}$ points as we show in Fig. (4).

C. Laser-induced spin & thermal Hall effects in CrI_3

The spin and thermal Hall effects are the hallmarks of topological insulating magnets. They determine the nature of spin excitations in magnetic insulators. For ordered magnets, it is believed that the spin and thermal Hall effects are a consequence of topological spin excitations in equilibrium systems [23–29, 64, 65]. In the non-equilibrium system, we consider the limit when the Bose occupation function is close to thermal equilibrium. Hence, a longitudinal temperature gradient $-\nabla_\beta T$ induces a transverse heat current $J_\alpha^Q = -\sum_\beta \kappa_{\alpha\beta} \nabla_\beta T$, where $\kappa_{\alpha\beta}$ is the thermal Hall conductivity [26] given by

$$\kappa_{\alpha\beta} = -k_B T \int_{BZ} \frac{d\mathbf{k}}{(2\pi)^3} \sum_{n=1}^N c_2[f_n^B(\mathbf{k})] \Omega_{n,\alpha\beta}(\mathbf{k}), \quad (17)$$

where $f_n^B(\mathbf{k}) = (e^{\varepsilon_n(\mathbf{k})/k_B T} - 1)^{-1}$ is the Bose occupation function close to thermal equilibrium, k_B the Boltzmann constant which we will set to unity, T is the temperature and $c_2(x) = (1+x) (\ln \frac{1+x}{x})^2 - (\ln x)^2 - 2\text{Li}_2(-x)$ weight function with $\text{Li}_2(x)$ being the dilogarithm.

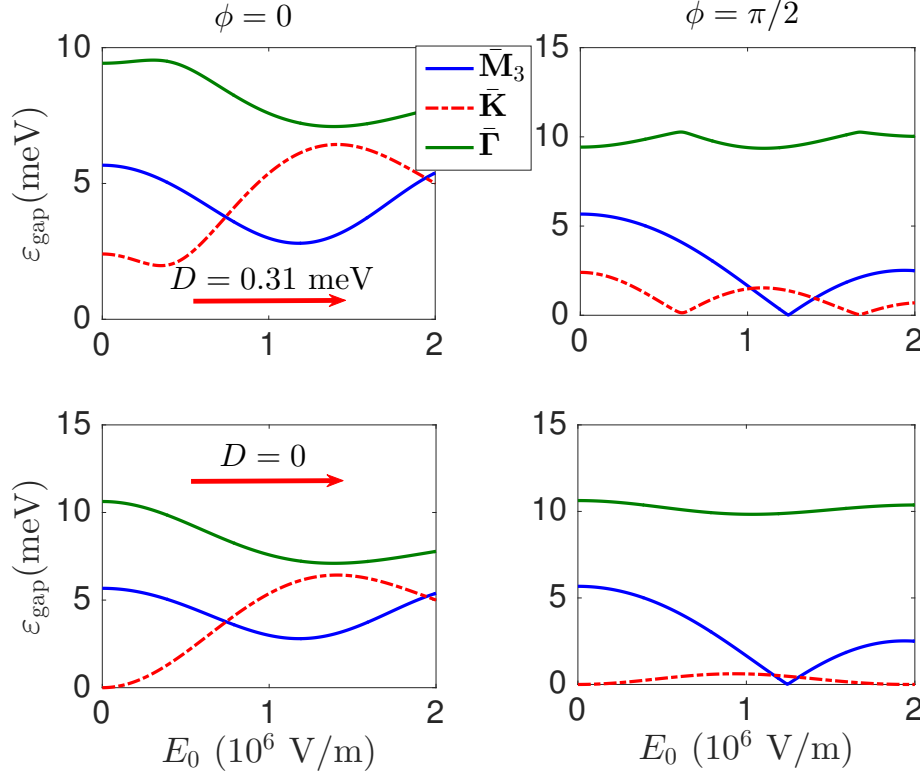


FIG. 4: Color online. The energy gap between the two Floquet topological magnon modes as a function of electric field intensity E_0 on the $k_z = 0$ plane for $\phi = 0$ left panel and $\phi = \pi/2$ right panel. The photon energy is $\hbar\omega = 30$ meV.

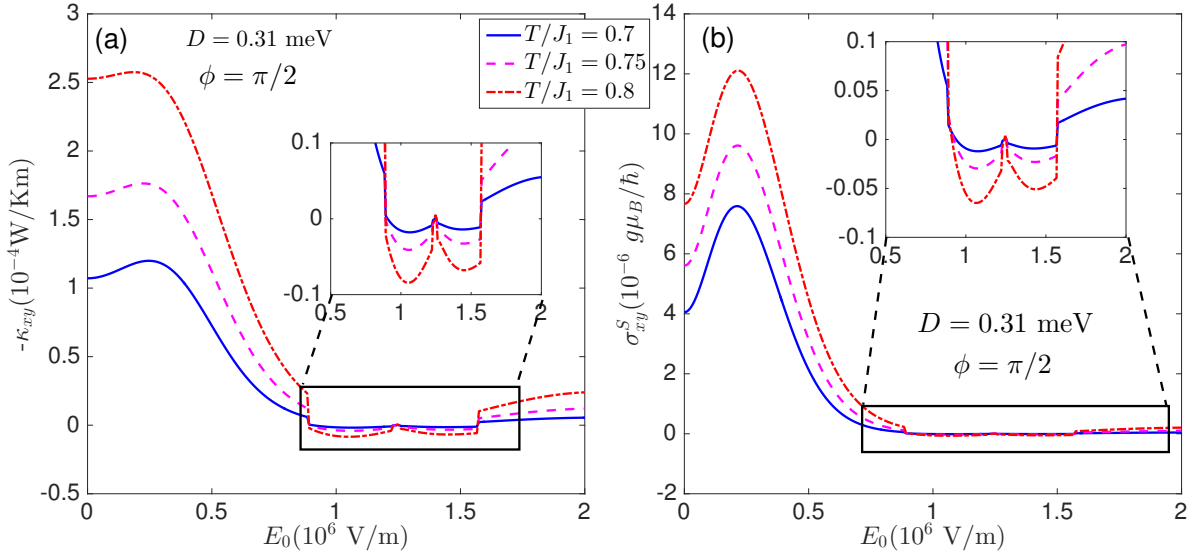


FIG. 5: Color online. Laser-induced spin and thermal Hall effects in CrI_3 as a function of E_0 for $\phi = \pi/2$ and various temperature values. Inset shows the magnified region (cf. Fig. (3)(b)).

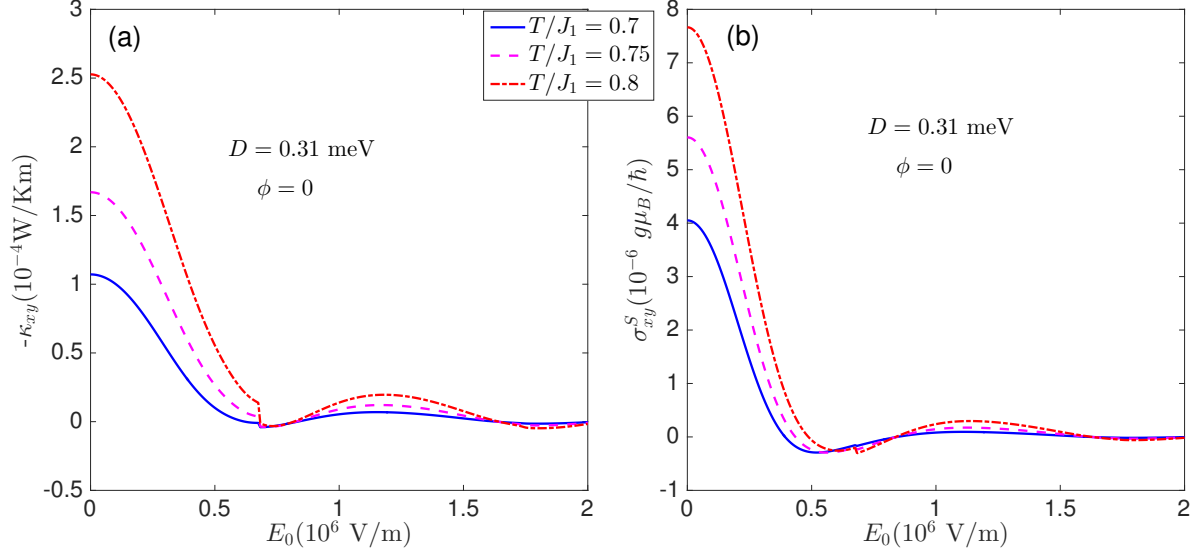


FIG. 6: Color online. Laser-induced spin and thermal Hall effects in CrI_3 as a function of E_0 for $\phi = 0$ and various temperature values.

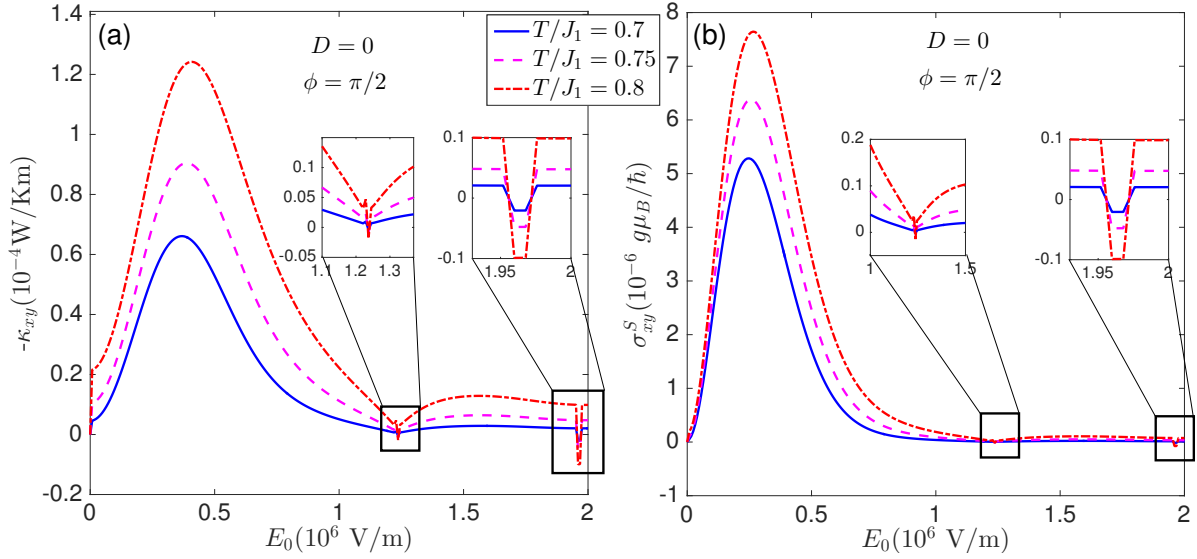


FIG. 7: Color online. Laser-induced spin and thermal Hall effects at zero DM interaction as a function of E_0 for $\phi = \pi/2$ and various temperature values. Inset shows the magnified region (cf. Fig. (3)(a)).

A magnetic field gradient $\nabla_\beta B^z$ can also induce a transverse spin current $J_\alpha^S = \sum_\beta \sigma_{\alpha\beta}^S \nabla_\beta B^z$, where $\sigma_{\alpha\beta}^S$ is the spin Hall conductivity [64, 65] given by

$$\sigma_{\alpha\beta}^S = \frac{g\mu_B}{\hbar} \int_{BZ} \frac{d\mathbf{k}}{(2\pi)^3} \sum_{n=1}^N f_n^B(\mathbf{k}) \Omega_{n,\alpha\beta}(\mathbf{k}), \quad (18)$$

In Fig. (5) and Fig. (6), we have shown the trends of the laser-induced spin σ_{xy}^S and thermal κ_{xy} Hall conductivities in CrI₃ for $\phi = \pi/2$ and $\phi = 0$ respectively. Note that the dimensionless Curie temperature of CrI₃ is $T_c/J_1 \sim 2.6$, hence the magnon bands are well-defined for $T < T_c$. Due to nonzero DM interaction, κ_{xy} and σ_{xy}^S are nonzero at equilibrium $E_0 = 0$ with κ_{xy} being negative. In the presence of a periodic drive $E_0 \neq 0$, there is a discernible change in both κ_{xy} and σ_{xy}^S as E_0 varies. In particular, for $\phi = \pi/2$, κ_{xy} and σ_{xy}^S first increase and reach a maximum peak before decreasing rapidly with increasing E_0 . At low temperature, there is a sign change in κ_{xy} and σ_{xy}^S for $\phi = \pi/2$, which coincides with the change of sign in the Chern number as shown in Fig. (3)(b). This shows that the magnon spin photocurrents can be switched by circularly-polarized laser field, which could pave the way towards opto-spintronics and opto-magnonics [1–10]. For $\phi = 0$, both κ_{xy} and σ_{xy}^S decrease rapidly with increasing E_0 . They eventually hit a bump where the Chern number (Berry curvature) changes to zero. However, they do not vanish completely in the regime of zero Chern number because of the bosonic nature of magnons. In other words, the Hall response is not a consequence of the Chern number in bosonic systems. It solely depends on the Berry curvature, which can be nonzero even when the Chern number is zero. In all cases, the Hall response becomes smaller after a topological phase transition. This is due to the change in the Berry curvature when the gap closes and reopens.

For zero DM interaction, κ_{xy} and σ_{xy}^S vanish at equilibrium $E_0 = 0$ and for $\phi = 0$ because time-reversal symmetry is not broken macroscopically. For $\phi = \pi/2$, however, time-reversal symmetry is broken and a nonzero κ_{xy} and σ_{xy}^S is manifested for $E_0 \neq 0$ as shown in Fig. (7). We can see that the sharp drop in κ_{xy} and σ_{xy}^S is consistent with the jump in the Chern number plot in Fig. (3)(a).

IV. CONCLUSION

In summary, we have showed that the spin and thermal Hall response in CrI₃ can be switched by a laser field. We also showed that photon-dressed topological phase transitions can occur in the spin wave excitations. The current results apply to both bulk and monolayer

CrI₃ with and without the DM interaction. A direct implication of the current results is that ultrafast spin photocurrents can be generated in CrI₃, which can be studied by the inverse Faraday effect. In addition, terahertz spectroscopy also provides a means to access the photon-dressed topological spin wave band structure in insulating magnets. Therefore, we have provided a platform for investigation of new features in CrI₃ and its potential applications to opto-spintronics, opto-magnonics, and magnon spintronics [1–10].

Appendix A: Floquet-Bloch theory

We implement the Floquet theory to study the periodically driven magnetic insulator CrI₃. Since the Hamiltonian is time-periodic we can expand it as

$$\mathcal{H}(\mathbf{k}, \tau) = \mathcal{H}(\mathbf{k}, \tau + T) = \sum_{n=-\infty}^{\infty} e^{in\omega\tau} \mathcal{H}_n(\mathbf{k}), \quad (\text{A1})$$

where

$$\mathcal{H}_n(\mathbf{k}) = \frac{1}{T} \int_0^T e^{-in\omega\tau} \mathcal{H}(\mathbf{k}, \tau) d\tau = \mathcal{H}_{-n}^\dagger(\mathbf{k}), \quad (\text{A2})$$

are the Fourier components and $T = 2\pi/\omega$ is the period of the laser light. The corresponding eigenvectors of the time-periodic Hamiltonian can be written as

$$|\psi_\alpha(\mathbf{k}, \tau)\rangle = e^{-i\varepsilon_\alpha(\mathbf{k})\tau} |u_\alpha(\mathbf{k}, \tau)\rangle, \quad (\text{A3})$$

where $|u_\alpha(\mathbf{k}, \tau)\rangle = |u_\alpha(\mathbf{k}, \tau + T)\rangle = \sum_n e^{in\omega\tau} |u_\alpha^n(\mathbf{k})\rangle$ is the time-periodic Floquet-Bloch wave function of magnon and $\varepsilon_\alpha(\mathbf{k})$ are the magnon quasienergy modes. We define the Floquet operator as $\mathcal{H}_F(\mathbf{k}, \tau) = \mathcal{H}(\mathbf{k}, \tau) - i\partial_\tau$.

The corresponding eigenvalue equation is of the form

$$\sum_m [\mathcal{H}_{n-m}(\mathbf{k}) + m\hbar\omega\delta_{n,m}] u_\alpha^m(\mathbf{k}) = \varepsilon_\alpha(\mathbf{k}) u_\alpha^n(\mathbf{k}), \quad (\text{A4})$$

where n, m are integers. The magnon quasienergies $\varepsilon_\alpha(\mathbf{k})$ can be obtained by diagonalizing the Floquet Hamiltonian

$$\mathcal{H}_F = \begin{pmatrix} \ddots & \vdots & \vdots & \vdots & \vdots \\ \cdots & \mathcal{H}_0 + \hbar\omega & \mathcal{H}_1 & \mathcal{H}_2 & \cdots \\ \cdots & \mathcal{H}_{-1} & \mathcal{H}_0 & \mathcal{H}_1 & \cdots \\ \cdots & \mathcal{H}_{-2} & \mathcal{H}_{-1} & \mathcal{H}_0 - \hbar\omega & \cdots \\ \vdots & \vdots & \vdots & \vdots & \ddots \end{pmatrix}. \quad (\text{A5})$$

Using the experimentally deduced parameters for CrI_3 [33], we obtain the magnon bandwidth of the undriven system \mathcal{H}_0 as $\Delta_{\mathbf{r}} = 6(J_1 + J_3)S = 19.71$ meV. When the photon energy $\hbar\omega$ is comparable to $\Delta_{\mathbf{r}}$, different copies of \mathcal{H}_0 overlap. However, when the photon energy $\hbar\omega$ is large compared to the magnon bandwidth $\Delta_{\mathbf{r}}$, the Floquet side modes are decoupled. We have considered the latter case. Thus, the system can be described by the effective time-independent Hamiltonian [41]

$$\mathcal{H}_{eff}(\mathbf{k}) = \mathcal{H}_0 + \sum_{n \geq 1} \frac{1}{n\hbar\omega} [\mathcal{H}_n, \mathcal{H}_{-n}] + \mathcal{O}\left(\frac{1}{\omega^2}\right). \quad (\text{A6})$$

-
- [1] Chumak, A. V. et al. Magnon spintronics. *Nat. Phys.* **11**, 453 (2015).
 - [2] Chumak, A. V., Serga, A. A. & Hillebrands, B. Magnon transistor for all-magnon data processing. *Nat. commun.* **5**, 4700 (2014).
 - [3] Khitun, A., Bao, M. & Wang, K. L. Magnonic logic circuits. *J. Phys. D: Appl. Phys.* **43**, 264005 (2010).
 - [4] Lenk, B. et al. The building blocks of magnonics. *Phys. Rep.* **507**, 107 (2011).
 - [5] Schellekens, A. J. et al. Ultrafast spin-transfer torque driven by femtosecond pulsed-laser excitation. *Nat. Commun.* **5**, 4333 (2014).
 - [6] Walowski J. & Münzenberg, M. Perspective: Ultrafast magnetism and THz spintronics. *J. Appl. Phys.* **120**, 140901 (2016).
 - [7] Nemec, P. et al. Antiferromagnetic opto-spintronics. *Nat. Phys.* **14**, 229 (2018).
 - [8] Satoh, T. et al. Spin Oscillations in Antiferromagnetic NiO Triggered by Circularly Polarized Light. *Phys. Rev. Lett.* **105**, 077402 (2010).
 - [9] Stanciu, C. D. et al. All-Optical Magnetic Recording with Circularly Polarized Light. *Phys. Rev. Lett.* **99**, 047601 (2007).
 - [10] Lenk, B. et al. Photo-magnonics. *arXiv:1208.5383* (2012).
 - [11] Huang, B. et al. Layer-dependent ferromagnetism in a van der Waals crystal down to the monolayer limit. *Nature* **546**, 270 (2017).
 - [12] Gong, C. et al. Discovery of intrinsic ferromagnetism in two-dimensional van der Waals crystals. *Nature* **546**, 265 (2017).

- [13] Zhong, D. et al. Van der Waals engineering of ferromagnetic semiconductor heterostructures for spin and valleytronics. *Sci. Adv.* **3**, e1603113 (2017).
- [14] Seyler, K. L. et al. Ligand-field helical luminescence in a 2D ferromagnetic insulator. *Nat. Phys.* **14**, 277 (2018).
- [15] Huang, B. et al. Electrical control of 2D magnetism in bilayer CrI₃. *Nat. Nanotechnol.* **13**, 544 (2018).
- [16] Jiang, S., Shan, J. & Mak, K. F. Electric-field switching of two-dimensional van der Waals magnets. *Nat. Mater.* **17**, 406 (2018).
- [17] Klein, D. R. et al. Probing magnetism in 2D van der Waals crystalline insulators via electron tunneling. *Science*, **360**, 1218 (2018).
- [18] Wang, Z. et al. Very large tunneling magnetoresistance in layered magnetic semiconductor CrI₃. *Nat. Commun.* **9**, 2516 (2018).
- [19] Lado J. L. & Rossier, J. F. On the origin of magnetic anisotropy in two dimensional CrI₃. *2D Mater.* **4**, 035002 (2017).
- [20] Dzyaloshinsky, I. A thermodynamic theory of "weak" ferromagnetism of antiferromagnetics. *J. Phys. Chem. Solids* **4**, 241 (1958).
- [21] Moriya, T. Anisotropic Superexchange Interaction and Weak Ferromagnetism. *Phys. Rev.* **120**, 91 (1960).
- [22] Owerre, S. A. A first theoretical realization of honeycomb topological magnon insulator. *J. Phys.: Condens. Matter* **28**, 386001 (2016).
- [23] Onose, Y. et al. Observation of the Magnon Hall Effect. *Science* **329**, 297 (2010).
- [24] Ideue, T. et al. Effect of lattice geometry on magnon Hall effect in ferromagnetic insulators. *Phys. Rev. B.* **85**, 134411 (2012).
- [25] Katsura, H., Nagaosa, N. & Lee, P. A. Theory of the Thermal Hall Effect in Quantum Magnets. *Phys. Rev. Lett.* **104**, 066403 (2010).
- [26] Matsumoto R. & Murakami, S. Theoretical Prediction of a Rotating Magnon Wave Packet in Ferromagnets. *Phys. Rev. Lett.* **106**, 197202 (2011).
- [27] Mook, A., Henk, J. & Mertig, I. Magnon Hall effect and topology in kagome lattices: A theoretical investigation. *Phys. Rev. B* **89**, 134409 (2014).
- [28] Hirschberger, M. et al. Thermal Hall Effect of Spin Excitations in a Kagome Magnet. *Phys. Rev. Lett.* **115**, 106603 (2015).

- [29] Owerre, S. A. Topological honeycomb magnon Hall effect: A calculation of thermal Hall conductivity of magnetic spin excitations. *J. Appl. Phys.* **120**, 043903 (2016).
- [30] Cramer, J. et al. Magnon detection using a ferroic collinear multilayer spin valve. *Nat. Commun.* **9**, 1089 (2018).
- [31] Rückriegel, A., Brataas, A. & Duine, R. A. Bulk and edge spin transport in topological magnon insulators. *Phys. Rev. B* **97**, 081106 (2018).
- [32] Proskurin, I. et al. Excitation of magnon spin photocurrents in antiferromagnetic insulators. *Phys. Rev. B* **98**, 134422 (2018).
- [33] Chen, L. et al. Topological Spin Excitations in Honeycomb Ferromagnet CrI_3 . *Phys. Rev. X* **8**, 041028 (2018).
- [34] Jin, W. et al. Raman fingerprint of two terahertz spin wave branches in a two-dimensional honeycomb Ising ferromagnet. *Nat. Commun.* **9**, 5122 (2018).
- [35] Oka, T. & Aoki, H. Photovoltaic Hall effect in graphene. *Phys. Rev. B* **79**, 081406 (2009).
- [36] Inoue, J. -I. & Tanaka, A. Photoinduced Transition between Conventional and Topological Insulators in Two-Dimensional Electronic Systems. *Phys. Rev. Lett.* **105**, 017401 (2010).
- [37] Lindner, N., Refael, G. & Gaslitiski, V. Floquet topological insulator in semiconductor quantum wells. *Nat. Phys.* **7**, 490 (2011).
- [38] Kitagawa, T. et al. Transport properties of nonequilibrium systems under the application of light: Photoinduced quantum Hall insulators without Landau levels. *Phys. Rev. B* **84**, 235108 (2011).
- [39] Wang, Y. H. et al. Observation of Floquet-Bloch States on the Surface of a Topological Insulator. *Science* **342**, 453 (2013).
- [40] Jotzu, G. et al. Experimental realization of the topological Haldane model with ultracold fermions. *Nature* **515**, 237 (2014).
- [41] Yan Z., & Wang, Z. Tunable Weyl Points in Periodically Driven Nodal Line Semimetals. *Phys. Rev. Lett.* **117**, 087402 (2016).
- [42] Chan, C. -K. et al. When Chiral Photons Meet Chiral Fermions: Photoinduced Anomalous Hall Effects in Weyl Semimetals. *Phys. Rev. Lett.* **116**, 026805 (2016).
- [43] Takasan, K., Nakagawa, M. & Kawakami, N. Laser-irradiated Kondo insulators: Controlling the Kondo effect and topological phases. *Phys. Rev. B* **96**, 115120 (2017).
- [44] Du, L. et al. Floquet topological transitions in extended Kane-Mele models with disorder.

- Phys. Rev. B **98**, 054203 (2018).
- [45] Hübener, H. et al. Creating stable Floquet-Weyl semimetals by laser-driving of 3D Dirac materials. Nat. Commun. **8**, 13940 (2017).
 - [46] Liu, H. et al. Photoinduced Nonequilibrium Topological States in Strained Black Phosphorus. Phys. Rev. Lett. **120**, 237403 (2018).
 - [47] McIver, J.W. et al. Light-induced anomalous Hall effect in graphene. arXiv:1811.03522.
 - [48] Rovillain, P. et al. Electric-field control of spin waves at room temperature in multiferroic BiFeO₃. Nature Mater. **9**, 975 (2010).
 - [49] Kirilyuk, A., Kimel, A. V. & Rasing, Th. Ultrafast optical manipulation of magnetic order. Rev. Mod. Phys. **82**, 2731 (2010).
 - [50] Vaz, C A F. Electric field control of magnetism in multiferroic heterostructures. J. Phys.: Condens. Matter **24**, 333201 (2012).
 - [51] Sato, M. , Takayoshi, S. & Oka, T. Laser-Driven Multiferroics and Ultrafast Spin Current Generation. Phys. Rev. Lett. **117**, 147202 (2016).
 - [52] Satoh, T. et al. Directional control of spin-wave emission by spatially shaped light. Nat. Photonics **6**, 662 (2012).
 - [53] Kimel, A. V. et al. Ultrafast non-thermal control of magnetization by instantaneous photo-magnetic pulses. Nature **435**, 655 (2005).
 - [54] Kampfrath, T. et al. Coherent terahertz control of antiferromagnetic spin waves. Nat. Photonics **5**, 31 (2011).
 - [55] Tzschaschel, C. et al. Ultrafast optical excitation of coherent magnons in antiferromagnetic NiO. Phys. Rev. B **95**, 174407 (2017).
 - [56] Owerre, S. A. Floquet topological magnons. J. Phys. Commun. **1**, 021002 (2017).
 - [57] Kar, S. & Basu, B. Photo-induced Entanglement in a Magnonic Floquet Topological Insulator. Phys. Rev. B **98** 245119 (2018).
 - [58] Elyasi, M., Sato, S. & Bauer G. E. W. Topologically nontrivial magnonic solitons. arXiv:1812.03738 (2018).
 - [59] Aharonov Y. & Casher, A. Topological Quantum Effects for Neutral Particles. Phys. Rev. Lett. **53**, 319 (1984).
 - [60] Stepanov, E. A., Dutreix, C. & Katsnelson, M. I. Dynamical and Reversible Control of Topological Spin Textures. Phys. Rev. Lett. **118**, 157201 (2017).

- [61] Claassen, M. et al. Dynamical time-reversal symmetry breaking and photo-induced chiral spin liquids in frustrated Mott insulators. *Nat. Commun.* **8**, 1192 (2017).
- [62] Hagen, C. R. Exact equivalence of spin-1/2 Aharonov-Bohm and Aharonov-Casher effects. *Phys. Rev. Lett.* **64**, 2347 (1990).
- [63] Chisnell, R. et al. Topological Magnon Bands in a Kagome Lattice Ferromagnet. *Phys. Rev. Lett.* **115**, 147201 (2015).
- [64] Fujimoto, S. Hall Effect of Spin Waves in Frustrated Magnets. *Phys. Rev. Lett.* **103**, 047203 (2009).
- [65] Lee, H., Han, J. H. & Lee, P. A. Thermal Hall effect of spins in a paramagnet. *Phys. Rev. B.* **91**, 125413 (2015).